PNAS RESEARCH ARTICLE | CELL BIOLOGY OPEN ACCESS

Non-cell-autonomous mechanisms of tumor initiation and relapse by chromosomal instability

Simona J. A. Lafirenze[a,b,1], Bastiaan van Gerwen[a,b,1], Ajit I. Quirindongo[a], Natasja Costermans[a,b], Aniek Janssen[c], Banafsheh Etemad[a,b], Pim Toonen[a,b], Marco A. D. Louro[a,b], Wilma H. M. Hoevenaar[a,b,2], Sameh Youssef[d], Alain de Bruin[d], Lodewijk A. A. Brosens[e], Nannette Jelluma[a,b,3], and Geert J. P. L. Kops[a,b,3,4]

Affiliations are included on p. 10.

Edited by David Pellman, Dana-Farber Cancer Institute, Boston, MA; received November 3, 2025; accepted May 14, 2026 by Editorial Board Member Rebecca Heald

Chromosomal instability (CIN) is a hallmark of cancer, and a primary cause of genetic heterogeneity in tumors. Depending on the degree of CIN and the affected tissue, CIN can promote or suppress tumor formation, and high CIN induction has been proposed as a therapeutic strategy. How CIN achieves these effects is unclear. Here we use a conditional mouse model of graded CIN in combination with longitudinal monitoring of DMBA/TPA-initiated skin tumors to show that low CIN increases the frequency of skin tumor initiation, while higher CIN accelerates tumor onset and growth rates. Strikingly, gene recombination analysis of the tumors reveals that upon high CIN induction the fast-growing tumors originate from rare low CIN cells, suggesting a strong non-cell-autonomous effect of high CIN. Gene expression analysis and immunohistochemistry show that high CIN causes epidermal hyperplasia, immune evasion, and a regenerative response that stimulates low CIN tumor growth beyond what is achieved by induction of low CIN alone. Such cell-extrinsic effects may be a common mechanism of tumor formation by CIN, as we observe it also in CIN-induced tumors of the intestine, breast, and mesentery. When high CIN is induced in established skin tumors, mimicking CIN-based therapy, tumors regress but relapse quickly. Relapsed tumors, too, arose from rare low CIN cells. Our findings have implications for our understanding of the contributions of CIN to cancer initiation and progression and give caution to the rationale for CIN therapies.

cancer | chromosomal instability | non-cell autonomous mechanism | inflammation

Significance

Chromosomal instability (CIN) is a source of genetic diversity in cancer. Different degrees of CIN can be highly oncogenic or tumor suppressive, the latter being a rationale for CIN-based cancer therapies. Using a mouse model for precise control of CIN levels, we find a) that the impact of the most oncogenic level of CIN on tumor formation is through effects on neighboring cells, by triggering a regenerative response accompanied by immune evasion, and b) that a similar response occurs upon induction of the very high CIN levels that are also induced by CIN-based therapies. CIN therefore has profound, indirect tumor-promoting effects on surrounding cells, which gives caution to the rationale for CIN therapies.

Aneuploidy is a hallmark of human tumors (1–3). Aneuploidy is caused by errors in chromosome segregation during cell division, the frequency of which is relatively high in human cancer cells (1, 4, 5). This phenotype, known as chromosomal instability (6), can drive tumor formation and progression, as well as have tumor suppressive effects (6–18). The mechanisms by which CIN promotes tumor formation and progression are not well understood. CIN results in chromosomal copy number alterations and can thereby promote gains of oncogenes or loss of tumor suppressor genes (19). CIN also creates micronuclei, which are a source of oncogenic genome rearrangements, gene amplification, and heritable epigenetic alterations to the micronucleated chromosomes (20–24). Besides these cell-intrinsic processes, CIN can cause non-cell-autonomous effects. Through generation of gene dosage imbalances and micronuclei, CIN can elicit innate immune responses that on the one hand promote immune surveillance and on the other hand drive IL6-dependent survival of CIN cells as well as immune evasion and metastatic cell behavior (11, 25–30). The pro- vs antitumor effects of CIN seem to depend on tissue context, degree of CIN, and duration of the CIN phenotype, all potentially influencing proliferation and survival as well as tumor microenvironmental and immune responses.The various consequences of CIN thus contribute to genome destabilization, intratumor heterogeneity, and tumor–immune interactions, which are thought to enable cancer cells to evolve new traits and adjust to their changing environment during growth, progression, and treatment (13, 26, 31–33).

Using a mouse model for CIN termed CiMKi (Cre-inducible *Mps1* Knock-in), we recently showed that the oncogenic potential of CIN depends on its level and location: moderate CIN is potently oncogenic in both small intestine and colon, but high CIN was so only in the colon (34). Very high CIN can however also be detrimental to tumors (10, 35). This spurred the notion that CIN could be used as therapy, in line with the effect of mainstay spindle poison therapies (e.g., paclitaxel). Indeed, several approaches to increase CIN in tumor treatments, for example by compromising the spindle assembly checkpoint

Author contributions: N.C., A.J., B.E., W.H.M.H., N.J., and G.J.P.L.K. designed research; S.J.A.L., B.v.G., A.I.Q., N.C., B.E., P.T., and W.H.M.H. performed research; S.J.A.L., M.A.D.L., S.Y., A.d.B., L.A.A.B., and N.J. analyzed data; and S.J.A.L., N.J., and G.J.P.L.K. wrote the paper.

The authors declare no competing interest.

This article is a PNAS Direct Submission. D.P. is a guest editor invited by the Editorial Board.

[1]S.J.A.L. and B.v.G. contributed equally to this work.

[2]Present address: Cancer Research UK Scotland Institute, Glasgow G61 1BD, United Kingdom.

[3]N.J. and G.J.P.L.K. contributed equally to this work.

[4]To whom correspondence may be addressed. Email: g.kops@hubrecht.eu.

This article contains supporting information online at https://www.pnas.org/lookup/suppl/doi:10.1073/pnas.2531095123/-/DCSupplemental.

Published June 17, 2026.

(36) or mitotic motor proteins, have been tested and are currently under investigation in clinical settings (reviewed in refs. 37 and 38) and see clinicaltrials.gov). Here we use our CiMKi model of conditional, graded CIN and a classic skin cancer model that enables longitudinal monitoring of growth dynamics to examine the mechanisms by which CIN contributes to initiation and growth of primary tumors as well its impact on preestablished tumors.

Results

Induction of Various Degrees of CIN in Skin. Our CiMKi mouse model for graded CIN allows tissue-specific induction of various degrees of CIN by conditional expression of different activity mutants of the master regulator of the SAC, the kinase Mps1. The resulting mutant combinations cause very low (WT/TA), low (WT/KD), moderate (TA/TA), high (TA/KD), and very high (KD/KD) CIN (Fig. 1*A*). To examine the contributions of CIN to tumor formation, we combined CiMKi with a classic carcinogenic model for cutaneous squamous cell carcinoma (cSCC), which enables accurate and longitudinal measurements of onset and growth of tumors after timed induction of various degrees of CIN. We previously showed that diverse degrees of CIN can be induced with our CiMKi model in mouse embryonic fibroblasts, in organoid cultures derived from colon and small intestine, and in the intestinal tissues (34). To verify its applicability for skin, we cultured skin organoids from normal, untreated dorsal skin (39) from *CiMKi;Rosa26-CreER*^{T2} mice (*SI Appendix*, Fig. S1), and introduced H2B-mNeon by lentivirus to enable live-imaging of chromosome segregation and quantification of CIN (*SI Appendix*, Fig. S2). Addition of 4-hydroxy-tamoxifen (4-OHT) to the organoids efficiently induced Cre-mediated recombination of the *CiMKi* alleles (*SI Appendix*, Fig. S1*C*). Live imaging of chromosome segregation showed that induction of the various CiMKi genotypes resulted in the same degrees of CIN (from very low to very high) as previously seen in the intestine (Fig. 1 *A* and *B*). Painting dorsal skin of *CiMKi;Rosa26-CreER*^{T2} mice with 4-OHT allowed for highly penetrant in vivo recombination of the *CiMKi* alleles specifically in the skin, as evidenced by undetectable signal of the wild-type nucleotide in the mutant codon position (Fig. 1*D*). We therefore conclude that our CiMKi model enables efficient induction of a range of CIN levels in the skin.

Different Degrees of CIN Have Distinct Effects on Skin Tumorigenesis. To examine the effects of various CIN levels on initiation and growth of skin tumors, we used the DMBA/TPA protocol for skin carcinogenesis on our *CiMKi;Rosa26-CreER*^{T2} mice (40). In this protocol, a single application of the chemical initiator mutagen DMBA (7,12-dimethylbenz[*a*]anthracene) causes tumor initiation through oncogenic *Hras* (41), while subsequent repeated treatment with the phorbol ester clonal expansion of initiating cells to papilloma or squamous cell carcinoma (SCC). The exact mechanism of the TPA contribution is not well understood but likely involves activation of PKC and an overall stimulation of proliferation, survival, and inflammation (42). We started biweekly application of TPA 7 d after DMBA treatment, followed by five single doses of 4-OHT on the backs of *CiMKi;Rosa26-CreER*^{T2} mice with all CiMKi genotypes (Fig. 2*A*). This resulted in markedly different effects on various aspects of tumorigenesis. First, moderate and higher CIN levels, but not the lower CIN levels, accelerated the appearance of the first tumors (early onset) (Fig. 2 *B–E* and *SI Appendix*, Fig. S2 *A* and *B*). Second, the moderate and higher CIN levels led to more large tumors indicative of increased tumor growth rates (43) (Fig. 2 *C* and *F* and *SI Appendix*, Fig. S2 *B–F*).

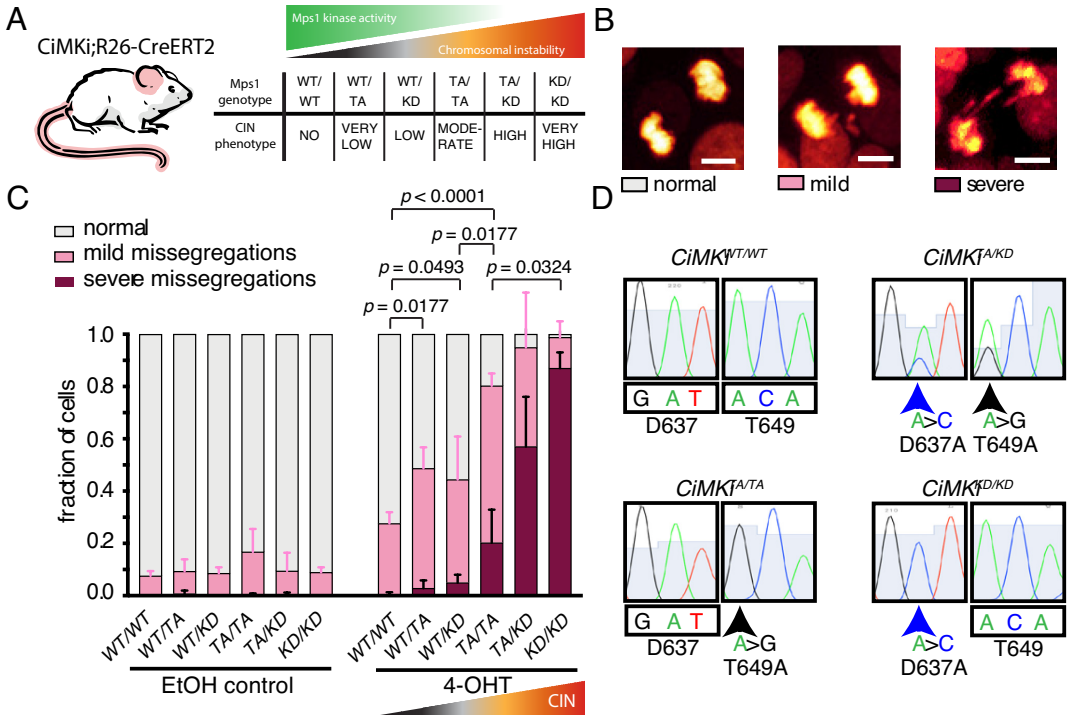

Fig. 1. Induction of various degrees of CIN in skin. (*A*) Schematic of the CiMKi mouse model. (*B*) Stills from timelapse movies of skin organoids of the *CiMKi;Rosa26-CreER*^{T2} genotypes 56 h after 4-OHT addition. DNA is visualized by H2B-mNeon. Chromosome segregation errors were categorized as indicated: severe (≥three), mild (one or two). See also Movies S1 and S2. (*C*) Quantification of chromosome segregation fidelity by time lapse imaging of skin organoids as in ref. 4. Means and error bars ± SEM of three independent organoid lines per genotype (at least 25 divisions per line and at least three individual organoids per line). *P*-values are for differences between the totals of segregation errors (mild plus severe): ordinary one-way ANOVA ($P < 0.0001$), followed by uncorrected Fisher's LSD test, exact *P*-values are indicated when $P < 0.05$. (*D*) Sequencing chromatograms of reverse transcribed RNA show efficient expression of both D637A (A to C) or T649A (A to G) CiMKi alleles in back skin of mice 1 wk after topical treatment with 4-OHT.

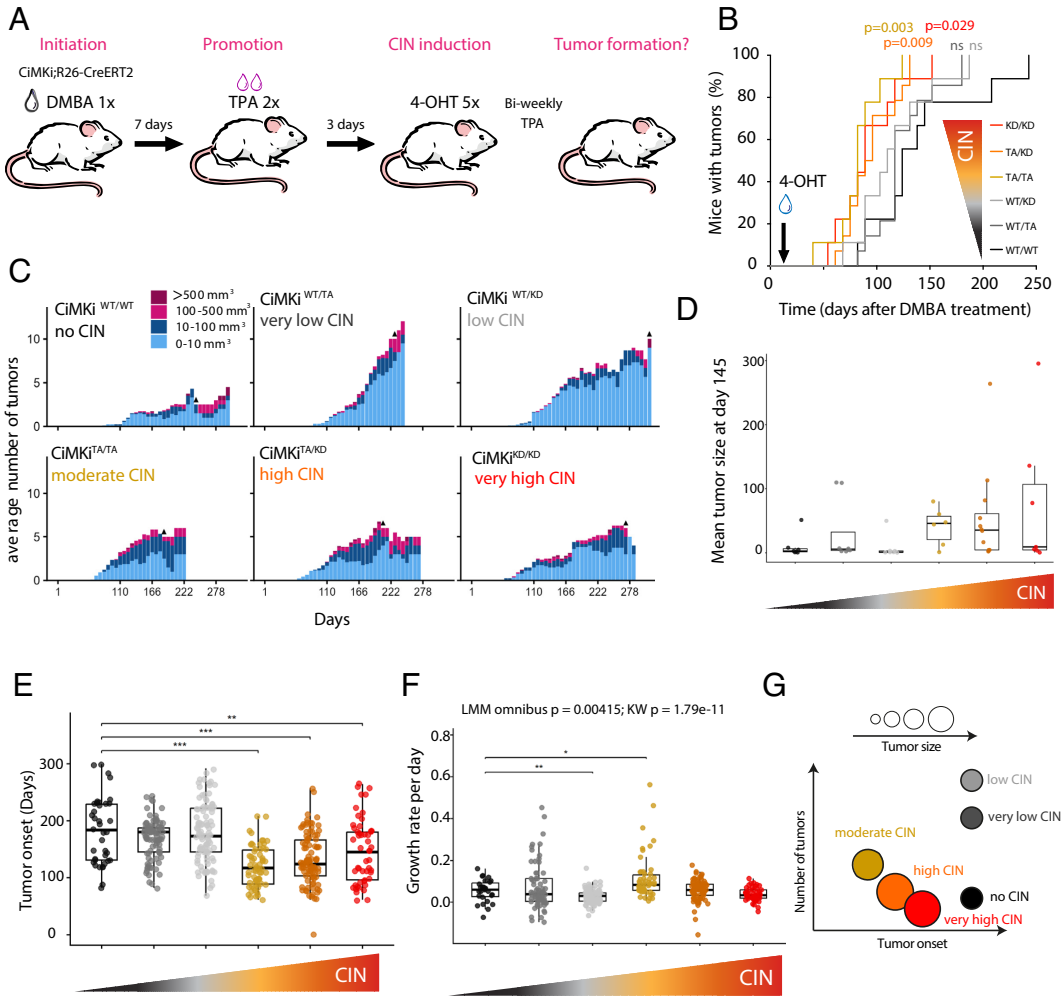

Fig. 2. Different degrees of CIN have distinct effects on skin tumorigenesis. (*A*) Treatment schedule of *CiMKi;Rosa26-CreER*^{T2} mice. Mice were topically treated as indicated. (*B*) Tumor incidence in *CiMKi;Rosa26-CreER*^{T2} mice treated as in (*A*). n = 9 (WT/WT, WT/KD, TA/TA), n = 14 (WT/TA, TA/KD), or n = 8 (KD/KD); *P*-values indicate significant differences of curves compared to WT/WT control curve (log-rank (Mantel-Cox) test). (*C*) Quantification of the average number and size of tumors in time in the *CiMKi;Rosa26CreER*^{T2} mice from *B* (4). Average tumor numbers were binned by size in four categories (0 to 10, 10 to 100, 100 to 500, and >500 mm^3) for each genotype. For tumors <10 mm, week-specific pairwise comparisons revealed that low CIN, was repeatedly associated with increased small-tumor burden relative to no CIN Triangle symbol on top of the bars indicates that only three mice are left after that timepoint. (*D*) Mean tumor size was calculated for each mouse at day 145 using only mice with at least one detectable tumor. Each dot represents one mouse, and boxplots show the median, interquartile range, and whiskers. Genotypes are shown on the x-axis. Overall differences between groups were assessed using a Kruskal–Wallis test (*P* = 0.0372). (*E*) Day of tumor onset is shown for tumors in control and CIN levels. Dots represent individual tumors; boxplots show median, interquartile range, and whiskers. Indicated pairwise comparisons are significant using a Kruskal–Wallis test (**P < 0.01, ***P < 0.001). (*F*) Exponential growth rates of individual tumors per day in the different genotypes. Each dot represents one tumor (minimum three timepoints required). Boxplots show median, interquartile range, and whiskers extend to 1.5× IQR. Significant pairwise comparisons vs. WT/WT are indicated (Kruskal–Wallis followed by the Dunn post hoc test with Benjamini–Hochberg correction; *P < 0.05, **P < 0.01). (*G*) Schematic representation of the distinct effects of the various CIN levels on tumorigenesis as shown in (*A*–*C*).

As a result, mice with moderate, high, and very high CIN levels experienced higher average total tumor volume as shown by their individual tumor volume curves (Fig. 2 *C* and *D* and *SI Appendix*, Fig. S2 *C* and *F*). End-point tumor grades were comparable between all CINlevels (*SI Appendix*, Fig. S2 *G* and *H*), but most mice from the moderate to very high CIN groups had to be sacrificed substantially earlier (Fig. 2*B*, triangles in Fig. 2*C* and *SI Appendix*, Fig. S2*F*). Third, very low, low, and moderate degrees of CIN substantially increased the total number of tumors per mouse as well as the average number of new tumors arising, whereas the higher degrees of CIN (high and very high) did so to a lesser extent (Fig. 2*C* and *SI Appendix*, Fig. S2 *E* and *D*). In summary (Fig. 2*G*): very low and low CIN levels affected predominantly the frequency with which tumors formed (number of tumors), high and very high CIN accelerated tumor onset and increased tumor size, and moderate CIN combined all these effects (higher numbers, larger size, and earlier onset).

Whole genome sequencing of three end-stage tumors from each CIN group showed distinct chromosomal copy number alterations specifically in tumors induced with moderate, high, and very high CIN. Most tumors from the WT group exhibited amplification of *Kras* and *Hras*-containing chromosomes 6 and 7 (44–47) (*SI Appendix*, Fig. S2*I*) probably due to the DMBA treatment. However, tumors from moderate, high, and very high CIN mice had additional whole chromosome alterations (e.g. gain of chromosome 16) that were absent from the lower CIN tumors or the WT tumors (*SI Appendix*, Fig. S2*I*). While these analyses cannot speak to CIN rates, the different effects of various CIN degrees on tumor initiation and growth were therefore accompanied by distinct whole chromosome gains.

Skin Tumors from High CIN Induction Arise from Low CIN Cells. Our results show that various degrees of CIN can have distinct effects on tumor initiation and growth, including

tumor-promoting effects of the highest CIN levels as a result of complete Mps1 inactivation (KD/KD). This was surprising, as we expected that very high CIN levels would be detrimental to cell viability. We therefore analyzed whether the tumor cells indeed carried fully recombined *CiMKi* alleles. For this, targeted Sanger sequencing for the *Mps1* point mutations was done on bulk cDNA obtained from mRNA from the tumors, and relative frequency of an allele was estimated based on relative peak intensities for the altered bases in the *Mps1* codons D367 and T649 (Fig. 3 *A* and *B*). Although not a quantitative measure, this provided an estimate of allele presence in the population, which sufficed for our purposes. Analysis of tumors that arose in skin of WT/TA and WT/KD mice expressed ~50% mutant Mps1 (*SI Appendix*, Fig. S3*A*), as expected from the efficient recombination seen in vivo (Fig. 1 *D*, *Bottom* panels). Surprisingly, however, only ~50% of *Mps1* mRNA molecules in tumors from KD/KD mice carried the KD mutation (Fig. 3*C*), showing that these tumors contained cells with unrecombined *CiMKi* alleles. We envisioned three scenarios to explain this: 1) either the tumors consisted of a mix of fully recombined tumor cells with nonrecombined cells (for example infiltrating immune cells); 2) the tumors consisted of cells in which only one allele had recombined; 3) a combination of the first and second scenarios. Our data strongly favor the second scenario: when tumors from TA/KD mice were analyzed, we found only one of the two CiMKi alleles in combination with WT, never both (Fig. 3*C*). If the WT allele had come from, e.g., immune infiltrate we should have found TA, KD, and WT alleles. Moreover, while recombination was initially very efficient for all genotypes when tested on healthy skin (no DMBA/TPA treatment) (Figs. 1*D* and 3*D* and *SI Appendix*, Fig. S3*B*), expression of one of the mutant alleles was lost over time in the TA/TA, TA/KD, and KD/KD mice (Fig. 3*D* and *SI Appendix*, Fig. S3*B*). We therefore conclude that moderate, high, and very high CIN cells are efficiently created in our model but are overtaken by rare cells in which only one allele had recombined and therefore had a low or very low CIN genotype (Fig. 3*E*). Yet, as shown in Fig. 2, the growth characteristics of these tumors were very different from those in which only one allele had recombined from the start (e.g., WT/TA or WT/KD).

Mammary, Intestinal, and Mesenteric Tumors After High CIN Induction Consist of Low CIN Cells. Intrigued by the observation that high CIN stimulates tumor forming capacity of rare low-CIN cells in the skin, we next wondered whether this also holds true for other tissues. To test this, we sequenced a variety of tumors from two studies in which high CIN also strongly promoted tumorigenesis: 1) intestinal and mammary tumors from $Apc^{Min/+}$; *Villin-Cre; TA/KD* mice (34), and 2) mesentery tumors from $p53^{lox/+}$; *Rosa26-CreERT2; TA/KD* or $p53^{+/+}$; *Rosa26-CreERT2; TA/KD* (*SI Appendix*, Fig. S3 *C* and *D*). For these tumors, we observed similar *Mps1* mutant allele expression patterns as we did for the skin tumors (Fig. 3*F*), indicating that, again, the tumor-forming cells had only a single recombined *CiMKi* allele instead of two. This suggests that in various tissues, induction of high CIN accelerates outgrowth of rare, low CIN tumor cells.

CIN Can Partially Substitute for TPA in the Skin Carcinogenesis Model. We next sought to better understand how high CIN can stimulate fast outgrowth of low CIN cells. Conditioned media from moderate CIN organoids or from apoptotic organoids did not significantly improve growth rates of low CIN organoids (*SI Appendix*, Fig. S4 *A*–*C*). A more complex, indirect mechanism might therefore be at play, and we wondered whether it may be inflammation (48). We therefore tested whether high CIN induction could replace TPA application in promoting tumorigenesis upon DMBA treatment. For this, *CiMKi;Rosa26-CreER*^{T2} mice were treated with one initiating dose of DMBA, after which various CIN levels were induced (Fig. 4*A*). While very low CIN did not impact tumorigenesis, induction of low CIN increased tumor burden. Moderate and high CIN accelerated and enhanced tumorigenesis by DMBA treatment (Fig. 4 *B* and *C*): tumors grew earlier and bigger, although the numbers of tumors were not as high as when TPA was used (see *Upper Left* panel of Fig. 2*C*). Very high CIN, while minimally affecting the number of tumors, caused tumors to grow larger and faster (Fig. 4 *B* and *C*) CIN levels could therefore, to an extent, substitute for TPA as a tumor promoter.

A Minor Role for Inflammation in Tumor Promotion by CIN. Whereas TPA has been reported to induce a plethora of processes, a notable one is inflammation, a known risk factor for cancer progression (48–51). To directly test the contribution of inflammation to the tumor-promoting effects of high CIN, we repeated the experiment in which we used moderate and high CIN to replace TPA, but now while treating the mice throughout the experiment with the nonsteroidal anti-inflammatory drug (NSAID) carprofen (Fig. 5*A*) (52). Immunohistochemistry confirmed that carprofen effectively inhibited CD45+ immune cell infiltration in TPA control and CIN-induced skin and skin tumors (Fig. 5 *E*–*G*). As expected, carprofen reduced the ability of TPA to promote tumor promotion after DMBA application (Fig. 5 *B* and *D*). Surprisingly, however, despite effective immune suppression, carprofen did not substantially reduce the number, size, or time of onset of tumors induced by DMBA and moderate CIN, and only marginally of tumors induced by DMBA and high CIN (Fig. 5 *C* and *D*). Although verification by an independent assay is needed for definitive conclusions, these results suggest that while inflammation may somewhat contribute to CIN-driven tumor promotion, it does not have a prominent role in our model.

Moderate/High CIN Promotes a Regenerative Tissue Response and Epidermal Hyperplasia. Our data imply that cells with high CIN, efficiently induced in our model, stimulate rare cells with low CIN to form tumors in a manner largely independent of inflammation. To identify the mechanism by which high CIN accomplishes this, we induced CIN in the skin for 1 and 4 wk, without DMBA/TPA application, and subsequently performed bulk RNA sequencing (53) (Fig. 6*A* and *SI Appendix*, Fig. S4*A*). Analysis of differentially expressed genes (DEGs) (54) revealed that 1 wk of CIN induction had caused an increase in keratinization and cellular proliferation, while fatty acid metabolism and cytokine expression were suppressed (Fig. 6*B* and *SI Appendix*, Fig. S4 *B*–*D*). A similar, albeit more pronounced, signature was seen 4 wk after CIN induction (Fig. 6*C* and *SI Appendix*, Fig. S4 *E* and *F*).

We next performed immunohistochemistry on skin tissues collected at the same timepoints. In line with the keratinization observed in the gene expression data, Masson's trichrome staining showed significant epidermal hyperplasia (acanthosis) in both moderate and high CIN groups, as seen by thickening of the epidermis, enlarged cells, and irregular nuclei, increased keratohyalin, and hyperkeratosis in all high CIN samples and in most moderate CIN samples (Fig. 6 *D* and *E*). All high CIN samples and the majority of moderate CIN samples exhibited hair follicle extension into adipose tissue, indicating anagen phase activation of hair growth, and this persisted after 4 wk (Fig. 6 *D* and *F* and *SI Appendix*, Fig. S4 *D*, *E*, *G*, and *H*). Furthermore, we observed signs of tissue regeneration: cells positive for PCNA or ki67 (proliferation), Gli1 and Gli2 (skin development and regeneration),

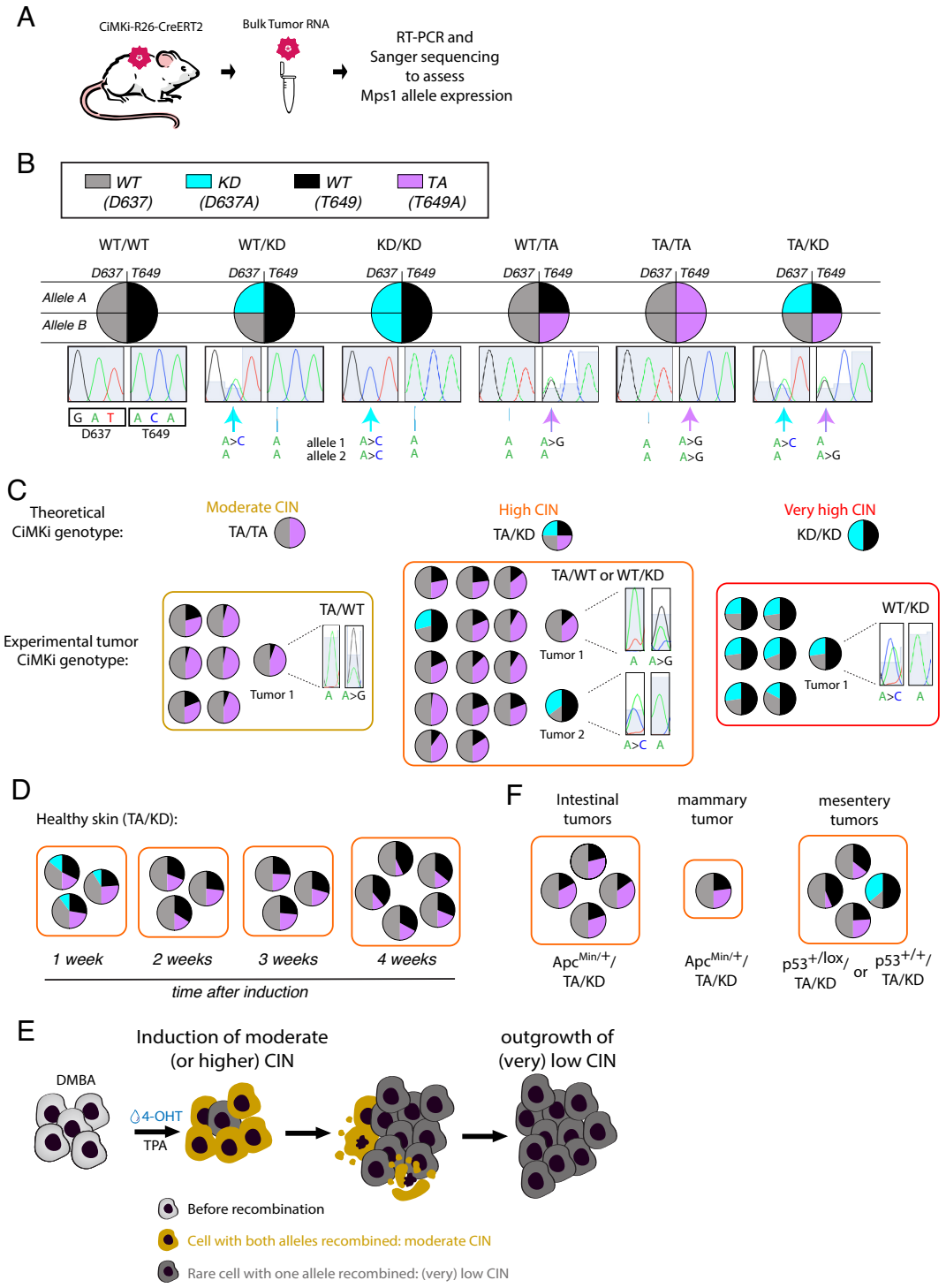

Fig. 3. Skin tumors from high CIN induction consist of low CIN cells. (*A*) Schematic representation of procedure: tumors are harvested from the back skin of the mice and RNA is extracted. RTPCR and Sanger sequencing follow to assess Mps1 allele expression. (*B*) Schematic to indicate the theoretical percentage of mutant expression per CiMKi allele (*A* and *B*) for the different CiMKi genotypes, when recombination is complete. In the example for TA/KD, allele A is recombined to D637A (KD) and thus WT for the T649 site (blue/black), and allele B is recombined to T649A and thus WT for the D637 site (purple/gray). Sequencing chromatograms of cDNA show typical examples of sequences of the two mutation sites when fully recombined (arrows indicated mutation). (*C*) Mutant expression in tumors from TA/TA (7 tumors), TA/KD (16 tumors), and KD/KD (7 tumors) mice. Notice the incomplete recombination of the Mps1 alleles in the tumors. (*D*) Mutant expression in healthy skin from TA/KD mice, 1, 2, 3, and 4 wk after induction. See *SI Appendix*, Fig. S3*B* for other *CiMKi* genotypes. (*E*) Mutant expression in method tumors and a mammary tumor from *Villin-Cre;* $Apc^{Min/+}$; TA/KD mice, and from mesentery tumors from *Rosa26-CreER^{T2};* $p53^{flox/+}$; TA/KD (1×) or *Rosa26-CreER^{T2};* $p53^{+/+}$; TA/KD mice (3×). In *B–D* the same color code was used as in *A*. (*F*) Moderate or higher CIN cells are efficiently created in CiMKi model after 4-OHT application, as detected by RTPCR and Sanger sequencing, indicating full recombination. However, in time these cells disappear and are overtaken by very rare, insufficiently recombined cells, in which only one allele had recombined and that therefore had a low or very low CIN genotype. These low CIN cells experience accelerated growth due to the microenvironment created by moderate/high CIN induction (Fig. 2*D*).

and SMA (fibroblast activation) were enriched in the suprabasal strata of the epidermis and partly in the hair follicle, exclusively in the moderate to very high CIN samples (Fig. 6 *F–H* and *SI Appendix*, Fig. S4 *I–N*). These enrichments may reflect a response to increased apoptosis induced by high CIN, as cleaved caspase-3 was detected in the basal epidermal layer of moderate

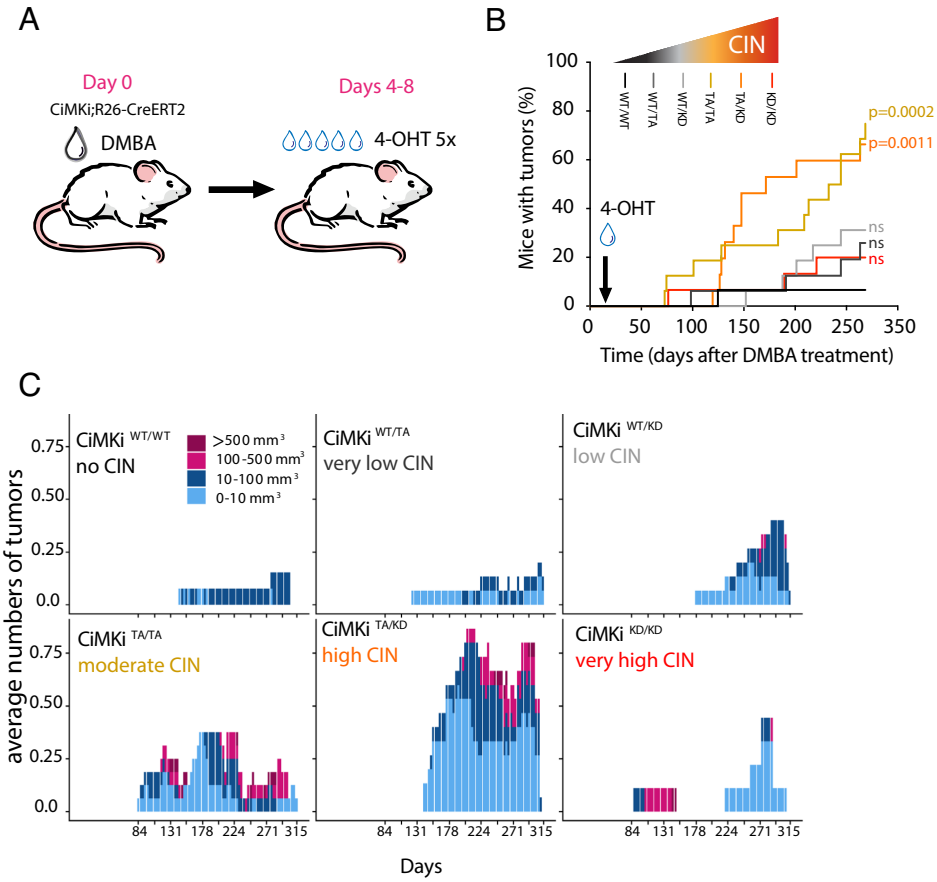

Fig. 4. CIN can substitute for TPA in the skin carcinogenesis model. (*A*) Treatment schedule of *CiMKi;Rosa26-CreER*^{T2} mice. Mice were topically treated on their back skin with DMBA (one dose), then with 4-OHT once a day for 5 consecutive days. (*B*) Tumor incidence in *CiMKi;Rosa26-CreER*^{T2} mice treated as in (*A*). *P*-values indicate significant differences of curves compared to WT/WT control curve (log-rank (Mantel-Cox) test). (*C*) Quantification of the average number and size of tumors in time in the *CiMKi;Rosa26CreER*^{T2} mice from (*B*). Average tumor numbers were binned by size in four categories (0 to 10, 10 to 100, 100 to 500, and >500 mm^3) for each genotype.

and high CIN samples but was rarely seen in the control (Fig. 6*L* and *SI Appendix*, Fig. S4*P*). In line with suppression of cytokines in the gene expression analysis, we found depletion of CD45+ cells in the tissue, indicative of immune evasion (Fig. 6 *M* and *N* and *SI Appendix*, Fig. S4*O*). The anagen growth and the regenerative response, accompanied by the absence of immune cells, continued after 4 wk from CIN induction (*SI Appendix*, Fig. S4 *E*, *G*, and *H*). These data suggest that induction of moderate to very high CIN levels (TA/TA, TA/KD, and KD/KD) in healthy skin triggers a proliferative and regenerative response that persist for weeks and leads to hyperplasia, which correlated with earlier tumor onset and enhanced tumor initiation and growth upon DMBA/TPA treatment (Fig. 2).

Tumor Relapse by Low CIN Cells After Regression from High CIN Induction. CIN induction is a therapeutic strategy for cancer (37, 46). Our data suggest that treatments that elevate CIN rates may have the unwanted consequence of promoting outgrowth of tumor cells with relatively low CIN. Since the DMBA/TPA model is well suited to monitor tumor growth longitudinally, we set out to test this by first establishing tumors by DMBA/TPA treatment of *CiMKi;Rosa26CreER*^{T2} mice and then subsequently inducing moderate, high, or very high CIN. When tumors reached a volume between 100 and 200 mm^3, they were painted with 4-OHT to recombine the *CiMKi* alleles and induce CIN (Fig. 7*A*). All three CIN levels led to initial regression of the skin tumors, the extent positively correlating with the degree of CIN induced (Fig. 7 *B* and *C* and *SI Appendix*, Fig. S5 *A* and *B*). Tumors relapsed after 1 to 7 wk after 4-OHT treatment (Fig. 7 *B* and *C*), with the exception of two out of 19 tumors that were challenged with very high CIN (*SI Appendix*, Fig. S5*B*, black lines in the KD/KD graph). Sequencing of *Mps1* cDNA again showed that relapsed tumors from KD/KD mice expressed ~50% of the KD mutation, and 50% wildtype Mps1 (7 out of 7) (Fig. 7*D*). Similarly, 4 out of 5 tumors from TA/KD mice expressed either the KD (2 out of 5) or TA (2 out of 5) mutation in a near 1:1 ratio with wildtype *Mps1* (Fig. 7*D*), and we even observed two tumors from the same TA/KD mouse in which one expressed only T649A and the other one only D637A (*SI Appendix*, Fig. S5*C*). Therefore, both during tumor promotion and tumor relapse, moderate, high, and very high CIN accelerate outgrowth of tumor cells with low CIN.

Discussion

We recently showed that the effects of CIN on intestinal tumorigenesis strongly depend on its degree and location along the intestinal tract (34). Here we assessed the effects of various CIN levels on tumor growth and regression dynamics, using the classic two-stage DMBA/TPA skin carcinogenesis model that enables facile longitudinal monitoring. In line with our study of intestinal tumorigenesis (34), the moderate level of CIN had the most profound impact, causing accelerated onset, increased frequency, and enhanced growth rates of the tumors. High and very high CIN accelerated tumor onset but did not enhance the number of tumors, while low and very low CIN only enhanced tumor numbers, not onset. Our present work again emphasizes the relevance of tissue and context on the impact of CIN on tumorigenesis: high CIN (TA/KD) does not promote tumorigenesis in the small intestine of *Apc*$^{Min/+}$ mice but does so in the large intestine (34), and, as we show here, high CIN is pro-tumorigenic also in the skin after DMBA and DMBA/TPA application. Moreover, while moderate and higher CIN levels alone (no other oncogenic treatment or mutation) could promote intestinal tumorigenesis, we did not observe any tumor formation in the 45 wk of experiment in the skin model.

What causes these different effects of CIN on tumorigenesis? Our data point to cell-intrinsic and -extrinsic effects that are differentially

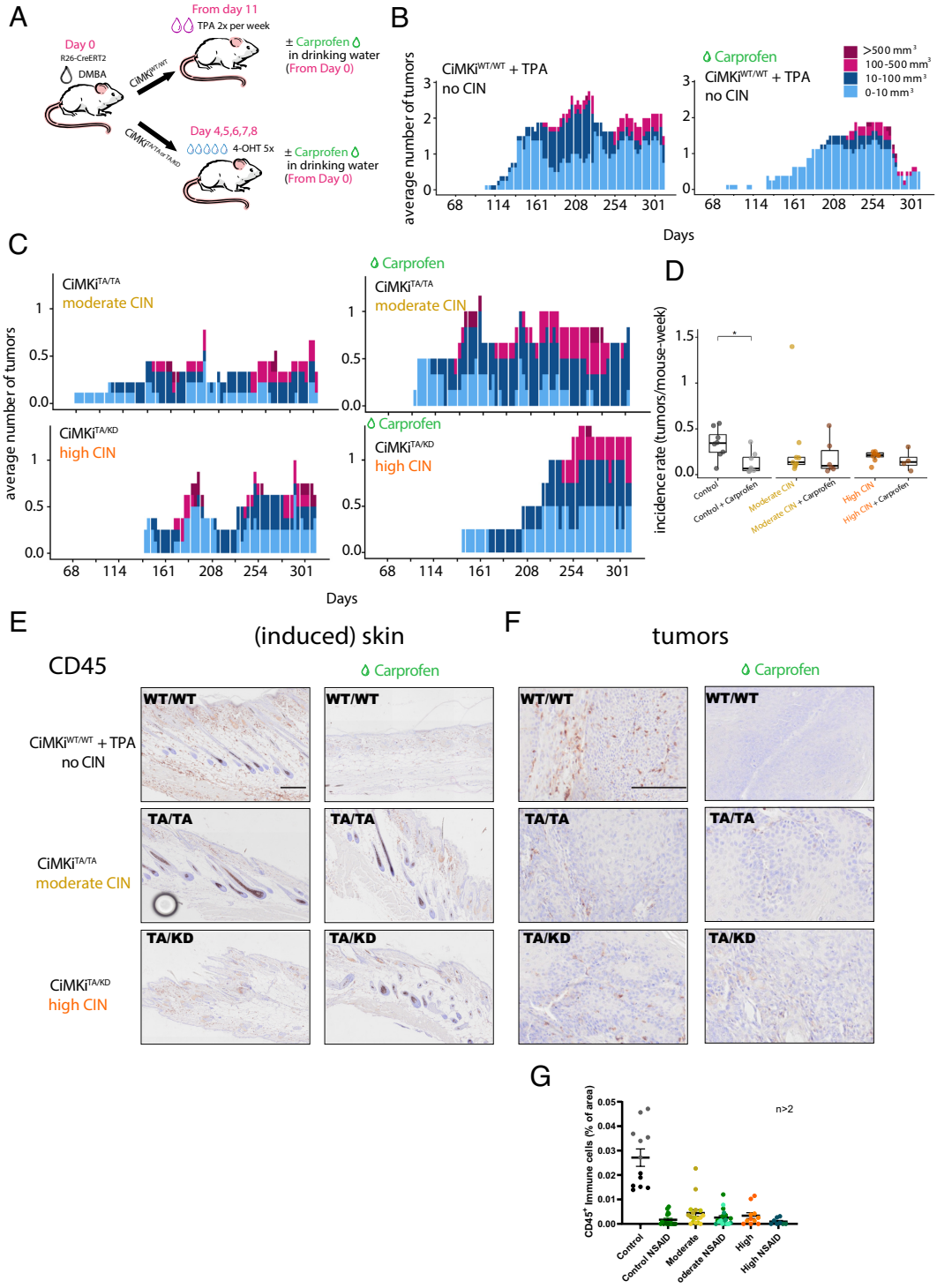

Fig. 5. A minor role for inflammation in tumor promotion by CIN. (*A*) Schematic representation of the experimental design: after DMBA application, no CIN (WT/WT) mice received biweekly treatment of TPA with or without carprofen in the water since the start of the experiment. These were taken along as a control for the effects of Carprofen. CIN (TA/TA and TA/KD) mice were treated with 4-OHT, after DMBA application, with or without carprofen in their drinking water. (*B*) Quantification of the average number and size of tumors in time in no CIN (WT/WT) mice treated as in Fig. 4*A*, but with having carprofen in their drinking water for the duration of the experiment. (*C*) Quantification of the average number and size of tumors in time in *CiMKi;Rosa26CreER*^{T2} moderate (TA/TA) and high (TA/KD) CIN mice treated as in Fig. 4*A*. Average tumor numbers were binned by size in four categories (0 to 10, 10 to 100, 100 to 500, and >500 mm^3) for each genotype. (*D*) Tumor incidence rate per mouse per week across genotypes and treatment conditions. Each dot represents one mouse. Boxes show median and interquartile range. Significance brackets indicate a statistically significant treatment effect within each genotype group (Wilcoxon rank-sum test, BH-adjusted). (*E*) Immunohistochemistry of CD45+cells in all CIN-induced skin and in carprofen treated conditions. (Scale bar, 100 μm.) (*F*) Decrease of immune (CD45+) cells in all carprofen treated conditions in induced tumors. (Scale bar, 1,000 μm.) (*G*) Quantification of CD45+ cells in induced tumors. Means and error bars ± SEM of three independent mice per genotype, except for control and high CIN which are two (five regions of interest randomly distributed along tumor regions per mouse).

induced by the various degrees of CIN. Besides copy number gains of chromosomes 6 and 7, common to the no-CIN tumors, tumors of all CIN genotypes were found to have other gains and losses, indicating that CIN increases the chance for the epithelial cells to reach an oncogenic karyotype, leading to a higher probability of tumor initiation and thus higher numbers of tumors. On the other

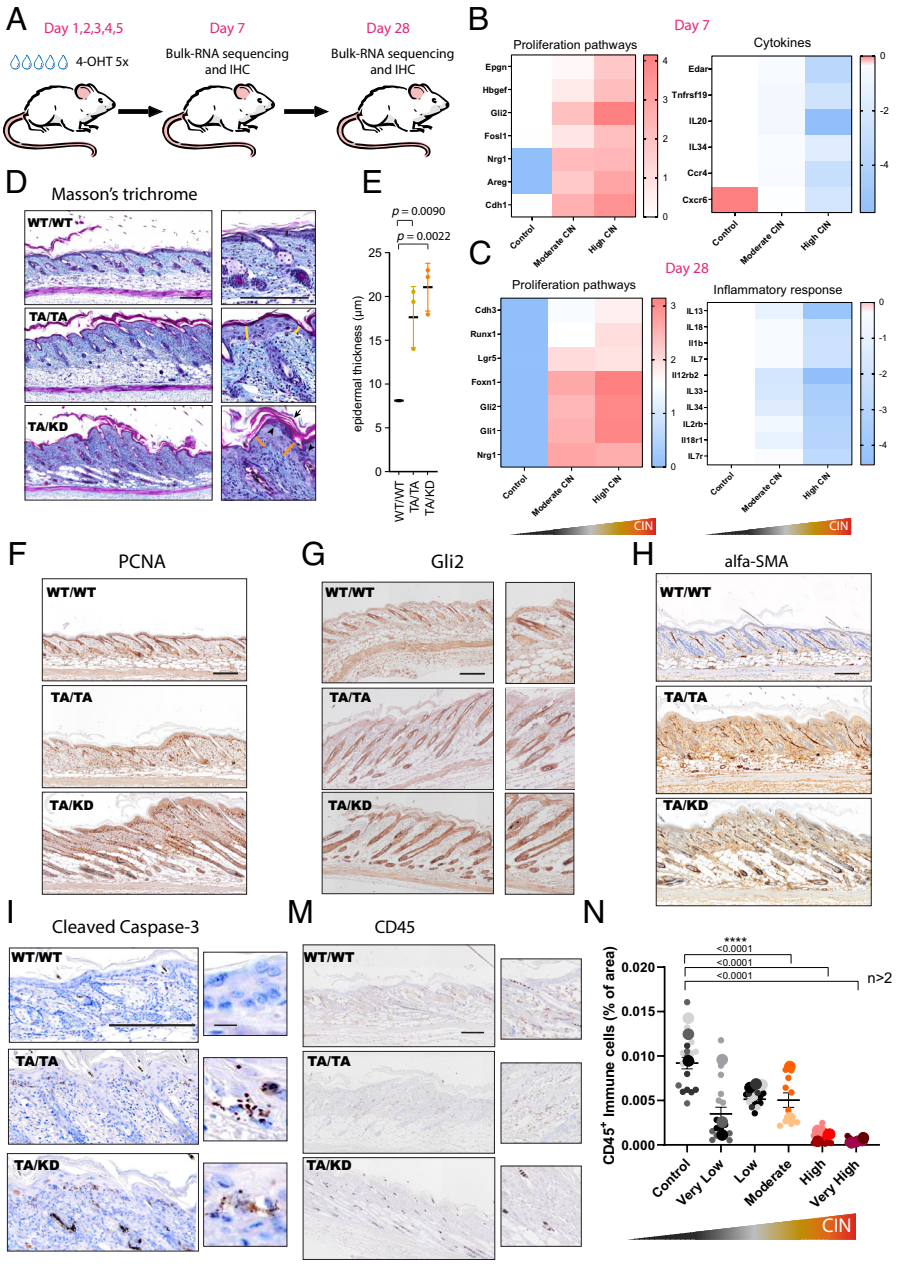

Fig. 6. Moderate/high CIN promotes a regenerative tissue response and epidermal hyperplasia. (*A*) Schematic representation of the experimental design: *CiMKi;Rosa26CreER*^{T2} (no CIN, moderate, and high CIN). Mice were topically treated on their back skin with 4-OHT once a day for 5 consecutive days. Skin tissues were harvested for bulk-RNA sequencing and for immunohistochemistry (IHC) at day 7 and at day 28 from CIN induction. (*B*) Heatmap (red up, blue down) showing expression of upregulated proliferation genes and downregulated expression of cytokines in high CIN compared to no CIN skin at day 7 from CIN induction. (*C*) Heatmap (red high, blue down) showing expression of upregulated proliferation genes and downregulated expression of inflammation in high CIN compared to no CIN skin at day 28 from CIN induction. (*D*) Masson's trichrome staining of mouse back skin 1 wk after induction of moderate (TA/TA) or high (TA/KD) CIN, or without induction of CIN (WT/WT). In the TA/KD sample large amounts of keratohyalin granules (*Inset*, arrowheads), and hyperkeratosis (*Inset*, arrow) is seen. Also, enlarged cells and irregular nuclei, and epidermal hyperplasia [acanthosis, straight lines in *Insets* indicate thickness of epidermis; see also (*B*)], are evident in both moderate and high CIN groups. In addition, we observed changes in the fibrotic structure (light blue staining) and signs of immune cell infiltration. (*E*) Measurement of epidermal thickness shows significant hyperplasia in the moderate and high CIN groups, compared to the WT/WT control. Means and error bars ± SEM of three independent mice per genotype (20 measurements randomly distributed along epidermis per mouse). *P*-values are for means: ordinary one-way ANOVA ($P < 0.0001$), followed by Tukey's multiple comparisons test, exact *P*-values are indicated when $P < 0.05$. (*F*) Increased proliferation in back skin 1 wk after induction of moderate (TA/TA) or high (TA/KD) CIN, as judged by PCNA staining: in controls (WT/WT), positive cells are nicely structured in 1 to 2 layers of suprabasal cells along the epidermis and hair follicles, while CIN samples show disorganization and a more random distribution of positive cells within the dermis and more than two positive cell layers in the epidermis. (*G*) Increased expression of Gli2 regenerative marker in all epithelial cells of the hair follicle (outer root sheath and dermal papilla) in moderate (TA/TA) and high (TA/KD) CIN samples compared to no CIN skin after 7 d from CIN induction. (Scale bars, 100 µm.) (*H*) Increased activated fibroblasts as judged by SMA staining in the back skin 1 wk after induction of moderate (TA/TA) or high (TA/KD) CIN: Compared to controls (WT/WT), more SMA positive signal is observed, in dermis and/or epidermis. (*I*) Increased apoptosis in the back skin 1 wk after induction of moderate (TA/TA) or high (TA/KD) CIN as judged by cleaved caspase 3 (CC3). Punctate patterns of CC3 staining is observed mostly below the basal layer of the epidermis (*Insets*), which are rarely observed in controls (WT/WT). (*M*) Decrease of CD45+ cells in moderate (TA/TA) and high (TA/KD) CIN skin compared to no CIN after 7 d from CIN induction. (*N*) Quantification of CD45+ cells in *CiMKi;Rosa26-CreER*^{T2}all ranges of CIN. Absence of CD45+ cells in all degrees of CIN, although to a bigger extent in high (TA/KD) and very high (KD/KD) CIN. Means and error bars ± SEM of three independent mice per genotype, except for moderate and very high which are two (six regions of interest randomly distributed along epidermis per mouse). *P*-values are for all datapoints from all replicates: ordinary one-way ANOVA ($P < 0.0001$) [Scale bars, 100 µm (*D* and *F–M*).]

hand, high and very high CIN tissue showed signs of increased cell death, immune evasion, and regeneration shortly after induction, suggesting additional cell-extrinsic effects of these high CIN levels (Fig. 8). This was further supported by the surprising finding that the fast-growing tumors after moderate/high CIN induction consisted of cells with low or very low CIN genotypes. This was true for tumors of the skin, the breast, the large intestine, and the mesentery, suggesting a more universal principle of non-cell-autonomous tumor promotion by high CIN. The fact that the tumors were uniformly of the same (very) low CIN genotype instead of mixed alleles shows that they most probably arose from a single clone. This is in line with recent data showing monoclonal origins of DMBA/TPA-induced SCC in mice (47). Given the observed high efficiency of recombination in vivo, assessed soon after induction, these data suggest that the fast disappearance of high CIN cells greatly stimulated survival and proliferation of very rare low CIN cells. Interestingly, in the tumors from moderate CIN (TA/KD) mice, very low CIN (WT/TA) cells grew out more often than low CIN (WT/KD) cells (*SI Appendix*, Fig. S3*B*), perhaps because the slightly more severe CIN (Fig. 1*C*) was more detrimental over time. The speed at which those rare cells grew to become a tumor is a striking example of strong non-cell-autonomous effects of high CIN on tumor formation. While we have not fully uncovered the mechanisms, our data suggest that inflammation does not play a major role: immune cells were mostly excluded from the tissue following CIN induction, and the NSAID carprofen did not substantially affect the impact of CIN on tumor promotion. This was unexpected, as CIN has known pro-inflammatory effects and we show it can supplant TPA as the

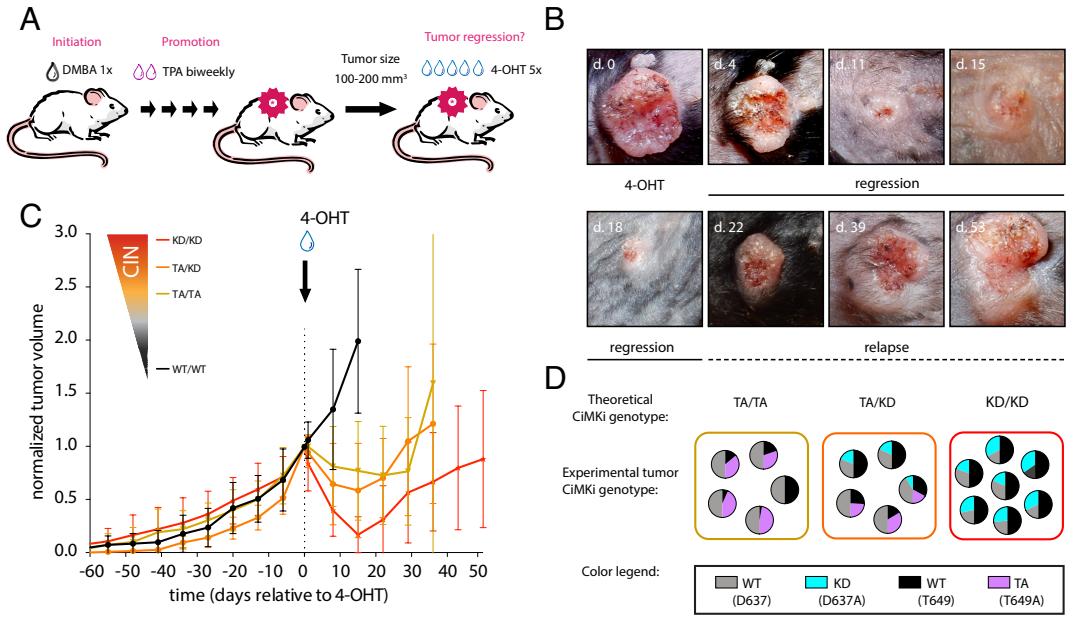

Fig. 7. Tumor size dynamics after high CIN induction as a therapy mimic. (*A*) Treatment schedule of *CiMKi; Rosa26-CreER*^{T2} mice. Mice were topically treated on their back skin with DMBA (one dose), and TPA (biweekly) to promote tumor formation, until the end of the experiment. Tumors sized 100-200 mm^3 were painted with 4-OHT on 5 consecutive days to induce the *CiMKi* alleles specifically in the tumors. (*B*) Example of a regressing and relapsing tumor in a *CiMKi*$^{KD/KD}$; *Rosa26-CreER*^{T2} after 4-OHT treatment: regression is instant, and almost complete at 18 d. Relapse is apparent 22 d after 4-OHT treatment (see also *SI Appendix*, Fig. S5*A*). (*C*) Average tumor volume plotted against time. Data are averages of different tumors (WT/WT (n = 8), TA/TA (n = 10), TA/KD (n = 7), KD/KD (n = 19). Volumes are relative to normalized volume at the start of 4-OHT treatment. Error bars indicate ± SD (see also *SI Appendix*, Fig. S5*B*). (*D*) Mutant expression in tumors from *CiMKi*$^{TA/TA}$, *CiMKi*$^{TA/KD}$, and *CiMKi*$^{KD/KD}$ mice.

promoting agent following initiation by DMBA. CIN and TPA therefore likely have other overlapping tumor-promoting mechanisms. The exact mechanism of the strong non-cell-autonomous oncogenic property of high CIN will be of great interest to uncover, as it might guide new therapeutic strategies.

Taken together, our data suggest that the differential effects of CIN on tumor initiation and growth originate from both cell-intrinsic and cell-extrinsic effects: the oncogenic cell-intrinsic effects of CIN (e.g., accelerated evolution of oncogenic karyotypes) are most efficiently sustained by low or very low CIN, causing increased initiation frequency, while oncogenic cell-extrinsic effects of CIN (e.g., a hyperregeneration response) are most efficiently created by higher CIN, speeding up growth. These effects are combined most optimally in the moderate CIN cells, causing acceleration of tumor onset, increase in initiation and increase in growth. Low and very low CIN lack the cell-extrinsic effect, resulting in predominantly accelerated onset. High and very high CIN cells eventually succumb, possibly due to unviable levels of aneuploidy, but leave a microenvironment ideal for rare low CIN cells to proliferate. This explains the accelerated onset and fast growth but lower number of tumors by (very) high CIN. It will be of great interest to untangle how the higher CIN levels cause the regenerative response, whether it is acute or chronic, and which features of the response have which effects on tumor initiation and growth.

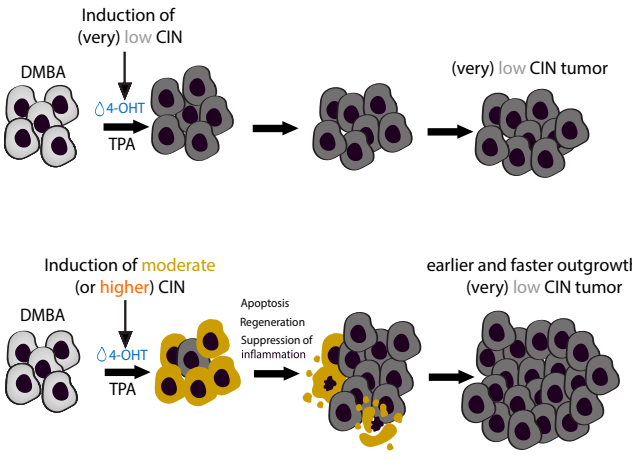

Fig. 8. Model for non-cell autonomous effects of high CIN levels in tumorigenesis. Moderate or higher CIN levels rapidly disappear from the tissue, possibly due to unviable levels of aneuploidy, but while doing so, they create a microenvironment ideal for rare low CIN cells to thrive. They induce a regenerative response accompanied by lack of immune cells and inflammation, which possibly explains the accelerated onset and fast growth but lower number of tumors by (very) high CIN. Low and very low CIN lack the cell-extrinsic effect, resulting only in increased tumor frequency.

The skin tumorigenesis model allowed for the monitoring of tumor size before and after CIN induction, which mimics therapeutic application of CIN-enhancing drugs such as microtubule poisons or inhibitors of mitotic kinases or kinesins (e.g., Aurora, MPS1, PLK1, Kif18A, or Kif11). We observed fast regression especially upon high and very high CIN induction. However, tumors relapsed quickly. Strikingly, the high CIN appeared to have promoted fast growth of rare low CIN cells, similar to the effects of high CIN during tumor initiation. Caution is therefore warranted when designing CIN-based therapeutic strategies. Optimizing the potential success of such strategies will require additional research into the mechanisms of the non-cell-autonomous effects of high CIN on tumor relapse.

Methods

Mice: Strains, Experiments, and Analysis. Animal experiments were approved by Animal Experimental Committee and the Dutch Central Authority for Scientific Procedures on Animals (CCD) and carried out in accordance with DIRECTIVE 2010/63/EU OF THE EUROPEAN PARLIAMENT AND OF THE COUNCIL. Animals were bred and housed under standard conditions (humidity 50 to 60%, 22 to 23 °C, inverted 12/12 h light/dark cycle, water, and standard chow ad libitum) at the animal facility of the Gemeenschappelijk Dieren Laboratorium (GDL), Utrecht,

the Netherlands, and the Hubrecht animal facility. Genetically modified mouse strains used in this study include: Cre-inducible-Mps1-Knock-in-TA (CiMKi^{TA}) and Cre-inducible-Mps1-Knock-in-KD (CiMKi^{KD}) (34) and available at JAX® (mice (B6.129P2(SJL)-*Ttk*$^{tm1.1Kops}$/JlmaJ (stock #035136) and B6.129P2(SJL)-*Ttk*$^{tm2.1Kops}$/JlmaJ (stock#035137), respectively), Rosa26-CreER^{T2} (purchased from JAX® mice (B6.129Gt(ROSA)26Sor$^{tm1(cre/ERT2)Tyj}$/J, stock#008463)), and p53^{LoxP} (purchased from JAX® mice (B6.129P2-*Trp53*^{tm1Brn}/J, stock#008462)). All mice were maintained in C57BL/6 background. For experiments involving p53 knock-out mice, *CiMKi; Rosa26-CreERT2; p53*$^{+/+}$ and *CiMKi; Rosa26-CreERT2; p53*$^{+/Flox}$ mice were generated. CIN and floxing of the p53 allele were induced by intraperitoneal injection with Tamoxifen (1 mg dissolved in corn oil; Sigma, C8267) when mice were 5 wk old. Mice were checked for general health and discomfort (according to the guidelines of the Dutch Code of Practice Animals in Cancer Research), weighed and palpated for the presence of tumors once a week. Mice were killed when a clear tumor could be palpated or when a humane endpoint was reached, or after maximally 104 wk. Whole body dissection was performed, and tissues and tumors were divided in two; and formalin fixed and embedded in paraffin, and snap-frozen in liquid nitrogen for further analyses. All mice were genotyped using standard PCR and targeted sequencing procedures (JAX® Mice and ref. 34, also see *SI Appendix*, Table S1).

Skin Tumorigenesis. For skin tumorigenesis experiments *CiMKi;Rosa26-CreERT2* of all CiMKi combinations were generated. To induce tumors, the classical DMBA/TPA skin carcinogenesis protocol (40) was followed, in combination with induction of various levels of CIN: back skin of 5- to 6-wk-old female mice was shaven and topically treated with a single dose of 7,12-dimethylbenz[a]-anthracene (DMBA) (800 nmol/0.2 mL acetone, Sigma). One week later, biweekly topical treatment of the back skin with 12-O-tetradecanoylphorbol-13-acetate (TPA) (4 μg/0.2 mL acetone, Sigma) started, for the duration of the experiment. CIN was induced 10 d after DMBA treatment by topical treatment on the back skin with 4-hydroxytamoxifen (4-OHT) (1 mg/0.2 mL DMSO, Sigma H6278) (five singles doses on consecutive days). To induce CIN at a later timepoint in established tumors (Fig. 7 and *SI Appendix*, Fig. S5), 4-OHT was applied in a similar way when tumors were 100 to 200 mm^3 in size. In case mice were treated with Carprofen (0.06 mg/mL, ProduLab Pharma BV) was added to the drinking water for the duration of the experiment. To monitor tumor growth, the backs of the mice were shaven as often as necessary and tumor volume was calculated by taking length and width measurements with a caliper every week. The average of these values was divided by two and taken as radius (volume = 4/3 π *r^3). Mice were euthanized when total tumor volume exceeded 1,500 mm^3, or maximally when 45 wk in experiment according to the approved procedure by the Animal Experimental Committee and the Dutch Central Authority for Scientific Procedures on Animals (CCD). At dissection, tumors, normal skin, and internal organs were isolated and divided to be snap-frozen or fixed in formalin. For identification and assessment of tumors 4-μm sections of paraffin-embedded tissue were cut and stained with hematoxylin/eosin (H&E). Grading of tumors was done by pathologists from the Dutch Molecular Pathology Centre.

Establishment and Culture of Skin Organoids. 3D organoids cultures were derived from back skins of 6- to 12-wk-old, culled *CiMKi;Apc*$^{Min/+}$*;Rosa26-CreER*^{T2} mice as described in ref. 39. See *SI Appendix* for complete media information.

Conditioned Media Experiment. Conditioned media (CM) was generated from intestinal organoid cultures carrying CiMKi alleles. See *SI Appendix* for complete media and details of procedure.

Assessment of CiMKi Mutant Allele Expression. To confirm recombination of the CiMKi alleles and mutant expression, RNA was isolated from tumors, normal skin, or skin organoids using the quick RNA kit (Zymo Research). cDNA was prepared using standard procedures, subjected to PCR and subsequently sequenced to determine the presence of T649A or D637A. For primers see *SI Appendix*, Table S1.

Histology and Immunohistochemistry. 4 to 5 μm sections of paraffin-embedded tissue were cut and stained with hematoxylin/eosin (H&E), or Masson's according to standard protocols. Antibodies details in *SI Appendix*.

Timelapse Microscopy. To analyze chromosome segregation using fluorescence microscopy time-lapse imaging, single cells that were cryopreserved immediately after collection were thawed and transduced with an H2B-Neon expressing lentivirus [pLV-H2B-mNeon-puro (34)]. For induction of CiMKi alleles organoids were treated with 1 μM 4-OHT for 56 h. Organoids were seeded 24 h before imaging in 8-chamber IBIDI slides and imaged with a confocal spinning disk (Nikon/Andor CSU-W1 with Borealis illumination), equipped with atmospheric and temperature control. Organoids were imaged in XYZT-mode (12 to 20 z-sections at 2.5 μm intervals, for 8 to 12 h) at 37 °C at 3-min intervals, using a 30X silicon objective and an additional 1.5X lens in front of the CCD-camera. 3% 448 nm laser and 50 nm disk pinhole were used. Raw data were converted to videos using a customized ImageJ/Fiji macro (36, 55). Fidelity of all observed chromosome segregations was scored and categorized manually, in a blinded manner.

Next Generation Sequencing. For bulk whole genome sequencing, genomic DNA was isolated from tumors and normal skin with the DNeasy Blood and Tissue kit (Qiagen) according to the manufacturer's instruction. Sequencing and copy number analysis were done at the Utrecht Sequencing Facility (useq.nl).

Bulk RNA Sequencing. Back skin of *CiMKi;Rosa26-CreER*^{T2} [no CIN, moderate (TA/TA) and high (TA/KD)] were treated with 4-hydroxytamoxifen (4-OHT) (1 mg/0.2 mL DMSO, Sigma H6278) (five singles doses on consecutive days) and were harvested 7 and 28 d after first application. RNA was isolated from the back skin of the mice using the Quick-RNA Tissue/Insect microprep kit (Zymo Research). More information about the procedure for the bulk-RNA sequencing can be found in *SI Appendix*.

Statistics and Data Reproducibility. Animals were randomized by combining various genotypes per cage. Treatments, tumor measurements, and analyses were done blinded. For mouse tumorigenesis and organoid studies, statistical analyses were done using GraphPad Prism. Data are presented as averages ± SD unless otherwise stated in legends. Statistical tests are indicated in the figure legends. Tumor growth was quantified by fitting log–linear models consistent with exponential growth to each individual tumor, from time of onset. Only tumors observed at three or more time points were included, as two points yield a perfectly determined line with no residual variance and therefore unreliable slope estimates. Tumor incidence rates were calculated as the number of newly arising tumors divided by the total observation time in mouse-weeks. Incidence rates were estimated per genotype either from the start of the experiment or from the time of first tumor onset, depending on the analysis. Genotype differences in tumor growth rates and incidence rates were assessed using Kruskal–Wallis tests followed by Dunn's post hoc pairwise comparisons against WT/WT, with p-values adjusted using the Benjamini–Hochberg method.

For supplementary material see *SI Appendix* and separate files containing Movies S1 and S2 and Dataset S1 for Fig. 3*C*.

Data, Materials, and Software Availability. The WGS and RNAseq data have been deposited in the European Nucleotide Archive database under the accession code PRJEB100986 (53). Non-cell-autonomous mechanisms of tumor initiation and relapse by chromosomal instability (https://github.com/Simo-Hub1/skin-tumor-analysis) (43). All other data are included in the manuscript and/or supporting information.

ACKNOWLEDGMENTS. We thank the Hubrecht animal facility, the Hubrecht Fluorescence-Activated Cell Sorting facility, the Hubrecht imaging facility, Single Cell Discoveries, and the Utrecht Sequencing Facilityfor assistance with the experiments. We thank Kim Boonekamp and Kai Kretschmar for support with skin organoid cultures, Harry Begthel, Jeroen Korving, and Jaimy Tatuhey for support with histology and stainings, and Dani Bodor for help with image processing. We thank Joana Fernandes Marques and Eugenio Marinelli for discussions about the data and for supporting energy levels during the rebuttal period. The Kops lab is part of Oncode Institute, which is partly funded by the Dutch Cancer Society (KWF Kankerbestrijding). This work was supported by the Dutch Cancer Society (Grant Nos. HUBR-2012-5321, HUBR-2012-5513, and KWF 10126) and by the European Research Council (ERC-SyG 855158).

Author affiliations: [a]Hubrecht Institute 3584 CT Koninklijke Nederlandse Akademie van Wetenschappen 1011 JV and University Medical Center Utrecht, Utrecht 3584 CX, The Netherlands; [b]Oncode Institute, Utrecht 3521 AL, The Netherlands; [c]Center for Molecular Medicine, University Medical Center Utrecht, Utrecht 3584 CX, The Netherlands; [d]Department of Biomolecular Health Sciences, Faculty of Veterinary Medicine, Utrecht University, Utrecht 3584 CL, The Netherlands; and [e]Department of Pathology, University Medical Center Utrecht, Utrecht 3584 CX, The Netherlands

1. R. H. van Jaarsveld, G. Kops, Difference makers: Chromosomal instability versus aneuploidy in cancer. *Trends Cancer* **2**, 561–571 (2016).
2. S. Heim, F. Mitelman, *Cancer Cytogenetics: Chromosomal and Molecular Genetic Aberrations of Tumor Cells* (Wiley-Liss Inc., New York, NY, ed. 2, 1995).
3. A. Kristin, T. D. Knouse, S. J. Elledge, A. Amon, Aneuploidy in cancer: Seq-ing answers to old questions. *Annu. Rev. Cancer Biol.* **1**, 335–354 (2017).
4. A. C. F. Bolhaqueiro *et al.*, Ongoing chromosomal instability and karyotype evolution in human colorectal cancer organoids. *Nat. Genet.* **51**, 824–834 (2019).
5. D. H. Bach, W. Zhang, A. K. Sood, Chromosomal instability in tumor initiation and development. *Cancer Res.* **79**, 3995–4002 (2019).
6. Ö. Serçin *et al.*, Transient PLK4 overexpression accelerates tumorigenesis in p53-deficient epidermis. *Nat. Cell Biol.* **18**, 100–110 (2016).
7. F. Foijer *et al.*, Chromosome instability induced by Mps1 and p53 mutation generates aggressive lymphomas exhibiting aneuploidy-induced stress. *Proc. Natl. Acad. Sci. U.S.A.* **111**, 13427–13432 (2014).
8. D. J. Baker, F. Jin, K. B. Jeganathan, J. M. van Deursen, Whole chromosome instability caused by Bub1 insufficiency drives tumorigenesis through tumor suppressor gene loss of heterozygosity. *Cancer Cell* **16**, 475–486 (2009).
9. L. S. Michel *et al.*, MAD2 haplo-insufficiency causes premature anaphase and chromosome instability in mammalian cells. *Nature* **409**, 355–359 (2001).
10. B. A. Weaver, A. D. Silk, C. Montagna, P. Verdier-Pinard, D. W. Cleveland, Aneuploidy acts both oncogenically and as a tumor suppressor. *Cancer Cell* **11**, 25–36 (2007).
11. S. F. Bakhoum *et al.*, Chromosomal instability drives metastasis through a cytosolic DNA response. *Nature* **553**, 467–472 (2018).
12. M. S. Levine *et al.*, Centrosome amplification is sufficient to promote spontaneous tumorigenesis in mammals. *Dev. Cell* **40**, 313–22.e5 (2017).
13. R. Sotillo *et al.*, Mad2 overexpression promotes aneuploidy and tumorigenesis in mice. *Cancer Cell* **11**, 9–23 (2007).
14. C. V. Rao *et al.*, Colonic tumorigenesis in BubR1+/-ApcMin/+ compound mutant mice is linked to premature separation of sister chromatids and enhanced genomic instability. *Proc. Natl. Acad. Sci. U.S.A.* **102**, 4365–4370 (2005).
15. R. M. Ricke, K. B. Jeganathan, J. M. van Deursen, Bub1 overexpression induces aneuploidy and tumor formation through Aurora B kinase hyperactivation. *J. Cell Biol.* **193**, 1049–1064 (2011).
16. M. Trakala *et al.*, Clonal selection of stable aneuploidies in progenitor cells drives high-prevalence tumorigenesis. *Genes Dev.* **35**, 1079–1092 (2021).
17. O. Shoshani *et al.*, Transient genomic instability drives tumorigenesis through accelerated clonal evolution. *Genes Dev.* **35**, 1093–1108 (2021).
18. Y. Iwanaga *et al.*, Heterozygous deletion of mitotic arrest-deficient protein 1 (MAD1) increases the incidence of tumors in mice. *Cancer Res.* **67**, 160–166 (2007).
19. V. Girish *et al.*, Oncogene-like addiction to aneuploidy in human cancers. *Science* **381**, eadg4521 (2023).
20. C. Z. Zhang *et al.*, Chromothripsis from DNA damage in micronuclei. *Nature* **522**, 179–184 (2015).
21. P. Ly *et al.*, Selective Y centromere inactivation triggers chromosome shattering in micronuclei and repair by non-homologous end joining. *Nat. Cell Biol.* **19**, 68–75 (2017).
22. P. Ly *et al.*, Chromosome segregation errors generate a diverse spectrum of simple and complex genomic rearrangements. *Nat. Genet.* **51**, 705–715 (2019).
23. S. Papathanasiou *et al.*, Heritable transcriptional defects from aberrations of nuclear architecture. *Nature* **619**, 184–192 (2023).
24. O. Shoshani *et al.*, Chromothripsis drives the evolution of gene amplification in cancer. *Nature* **591**, 137–141 (2021).
25. J. Li *et al.*, Non-cell-autonomous cancer progression from chromosomal instability. *Nature* **620**, 1080–1088 (2023).
26. S. F. Bakhoum, L. C. Cantley, The multifaceted role of chromosomal instability in cancer and its microenvironment. *Cell* **174**, 1347–1360 (2018).
27. C. Hong *et al.*, cGAS–STING drives the IL-6-dependent survival of chromosomally instable cancers. *Nature* **607**, 366–373 (2022).
28. A. Brink, M. F. Suárez Peredo Rodríguez, F. Foijer, Chromosomal instability and inflammation: A catch-22 for cancer cells. *Chromosom. Res.* **31**, 19 (2023).
29. R. W. Wang, S. Viganò, U. Ben-David, A. Amon, S. Santaguida, Aneuploid senescent cells activate NF-κB to promote their immune clearance by NK cells. *EMBO Rep.* **22**, e52032 (2021).
30. T. Davoli, H. Uno, E. C. Wooten, S. J. Elledge, Tumor aneuploidy correlates with markers of immune evasion and with reduced response to immunotherapy. *Science* **355**, eaaf8399 (2017).
31. R. A. Burrell, N. McGranahan, J. Bartek, C. Swanton, The causes and consequences of genetic heterogeneity in cancer evolution. *Nature* **501**, 338–345 (2013).
32. L. Sansregret, B. Vanhaesebroeck, C. Swanton, Determinants and clinical implications of chromosomal instability in cancer. *Nat. Rev. Clin. Oncol.* **15**, 139–150 (2018).
33. D. A. Lukow, J. M. Sheltzer, Chromosomal instability and aneuploidy as causes of cancer drug resistance. *Trends Cancer* **8**, 43–53 (2022).
34. W. H. M. Hoevenaar *et al.*, Degree and site of chromosomal instability define its oncogenic potential. *Nat. Commun.* **11**, 1501 (2020).
35. A. D. Silk *et al.*, Chromosome missegregation rate predicts whether aneuploidy will promote or suppress tumors. *Proc. Natl. Acad. Sci. U.S.A.* **110**, E4134–E4141 (2013).
36. J. Drost *et al.*, Sequential cancer mutations in cultured human intestinal stem cells. *Nature* **521**, 43–47 (2015).
37. L. L. Thompson, L. M. Jeusset, C. C. Lepage, K. J. McManus, Evolving therapeutic strategies to exploit chromosome instability in cancer. *Cancers* **9**, 151 (2017).
38. S. F. Bakhoum, D. A. Compton, Chromosomal instability and cancer: A complex relationship with therapeutic potential. *J. Clin. Invest.* **122**, 1138–1143 (2012).
39. K. E. Boonekamp *et al.*, Long-term expansion and differentiation of adult murine epidermal stem cells in 3D organoid cultures. *Proc. Natl. Acad. Sci. U.S.A.* **116**, 14630–14638 (2019).
40. E. L. Abel, J. M. Angel, K. Kiguchi, J. DiGiovanni, Multi-stage chemical carcinogenesis in mouse skin: Fundamentals and applications. *Nat. Protoc.* **4**, 1350–1362 (2009).
41. H. Fujiki *et al.*, Codon 61 mutations in the c-Harvey-ras gene in mouse skin tumors induced by 7,12-dimethylbenz[a]anthracene plus okadaic acid class tumor promoters. *Mol. Carcinog.* **2**, 184–187 (1989).
42. A. G. R. Rachana Garg, G. B. Maru, Curcumin decreases 12-O-tetradecanoylphorbol-13-acetate–induced protein kinase C translocation to modulate downstream targets in mouse skin. *Carcinogenesis* **29**, 1249–1257 (2008).
43. S. J. A. Lafirenze *et al.*, Non-cell-autonomous mechanisms of tumor initiation and relapse by chromosomal instability. GitHub. https://github.com/Simo-Hub1/skin-tumor-analysis. Deposited 13 April 2026.
44. C. M. Aldaz, D. Trono, F. Larcher, T. J. Slaga, C. J. Conti, Sequential trisomization of chromosomes 6 and 7 in mouse skin premalignant lesions. *Mol. Carcinog.* **2**, 22–26 (1989).
45. M. D. To *et al.*, Progressive genomic instability in the FVB/Kras(LA2) mouse model of lung cancer. *Mol. Cancer Res.* **9**, 1339–1345 (2011).
46. R. Hosea, S. Hillary, S. Naqvi, S. Wu, V. Kasim, The two sides of chromosomal instability: Drivers and brakes in cancer. Signal Transduct. *Target Ther.* **9**, 75 (2024).
47. M. Q. Reeves, E. Kandyba, S. Harris, R. Del Rosario, A. Balmain, Multicolour lineage tracing reveals clonal dynamics of squamous carcinoma evolution from initiation to metastasis. *Nat. Cell Biol.* **20**, 699–709 (2018).
48. J. E. Rundhaug, S. M. Fischer, Molecular mechanisms of mouse skin tumor promotion. *Cancers* **2**, 436–482 (2010).
49. G. B. Maru, K. Gandhi, A. Ramchandani, G. Kumar, The role of inflammation in skin cancer. *Adv. Exp. Med. Biol.* **816**, 437–469 (2014).
50. L. M. Coussens, Z. Werb, Inflammation and cancer Nature. **420**, 860–867 (2002).
51. M. Neagu *et al.*, Inflammation: A key process in skin tumorigenesis. *Oncol. Lett.* **17**, 4068–4084 (2019).
52. J. C. Ingrao *et al.*, Aqueous stability and oral pharmacokinetics of meloxicam and carprofen in male C57BL/6 mice. *J. Am. Assoc. Lab. Anim. Sci.* **52**, 553–559 (2013).
53. S. J. A. Lafirenze *et al.*, Non-cell-autonomous mechanisms of tumor initiation and relapse by chromosomal instability. European Nucleotide Archive Database. https://www.ebi.ac.uk/ena/browser/text-search?query=PRJEB100986. Deposited 1 April 2026.
54. M. I. Love, W. Huber, S. Anders, Moderated estimation of fold change and dispersion for RNA-seq data with DESeq2. *Genome Biol.* **15**, 550 (2014).
55. C. S. Verissimo *et al.*, Targeting mutant RAS in patient-derived colorectal cancer organoids by combinatorial drug screening. *eLife* **5**, e18489 (2016).